9-26-2017

A Stimulated Emission Study of the Ground State Bending Levels of BH_2 Through the Barrier to Linearity and *Ab Initio* Calculations of Near-Spectroscopic Accuracy

Bing Jin
University of Kentucky

Dennis J. Clouthier
University of Kentucky, dclaser@uky.edu

Riccardo Tarroni
Universita di Bologna, Italy

A Stimulated Emission Study of the Ground State Bending Levels of BH_2 Through the Barrier to Linearity and *Ab Initio* Calculations of Near-Spectroscopic Accuracy

Digital Object Identifier (DOI)
https://doi.org/10.1063/1.4990760

A stimulated emission study of the ground state bending levels of BH_2 through the barrier to linearity and ab initio calculations of near-spectroscopic accuracy

Bing Jin, Dennis J. Clouthier, and Riccardo Tarroni

Citation: The Journal of Chemical Physics **147**, 124303 (2017); doi: 10.1063/1.4990760
View online: https://doi.org/10.1063/1.4990760
View Table of Contents: http://aip.scitation.org/toc/jcp/147/12
Published by the American Institute of Physics

A stimulated emission study of the ground state bending levels of BH_2 through the barrier to linearity and *ab initio* calculations of near-spectroscopic accuracy

Bing Jin,[1] Dennis J. Clouthier,[1,a)] and Riccardo Tarroni[2]
[1]*Department of Chemistry, University of Kentucky, Lexington, Kentucky 40506-0055, USA*
[2]*Dipartimento di Chimica Industriale "Toso Montanari," Universita di Bologna, Viale Risorgimento 4, 40136 Bologna, Italy*

(Received 17 June 2017; accepted 6 September 2017; published online 26 September 2017)

The ground state bending levels of $^{11}BH_2$ have been studied experimentally using a combination of low-resolution emission spectroscopy and high-resolution stimulated emission pumping (SEP) measurements. The data encompass the energy range below, through, and above the calculated position of the barrier to linearity. For the bending levels (0,3,0) and above, the data show substantial K-reordering, with the $K_a'' = 1$ levels falling well below those with $K_a'' = 0$. A comparison of the high-resolution rotationally resolved SEP data to our own very high level *ab initio* calculations of the rovibronic energy levels shows agreement approaching near-spectroscopic accuracy (a few cm^{-1}). The data reported in this work provide very stringent tests for future theoretical treatments of this prototypical seven-electron free radical. *Published by AIP Publishing.* https://doi.org/10.1063/1.4990760

I. INTRODUCTION

With only seven electrons, BH_2 is one of the "simplest" known polyatomic molecules,[1] eclipsed only by trihydrogen (H_3)[2] and beryllium dihydride (BeH_2).[3] The boron dihydride radical was first reported by Herzberg and Johns[1] in 1967 through observation of the gas phase electronic spectrum obtained by flash photolysis of borane carbonyl (BH_3CO). In their pioneering work, the authors proved that the observed electronic transition is between the two components of what would be a $^2\Pi$ state at linearity. The data showed that BH_2 is a bent near-prolate asymmetric top in the lower state and adopts a linear structure in the excited state. The observed $^{11}BH_2$ spectra spanned the 11 500–15 400 cm^{-1} region, initially assigned to the 2_0^7 through 2_0^{11} vibronic transitions (ν_2 is the bending vibration). Spin splittings were observed in only one sub-band Δ–Π of 2_0^7, establishing the doublet nature of the states but providing little information on the ground or excited state spin splittings. A few bands of $^{10}BH_2$ and $^{11}BD_2$ were also identified, and the isotope effects were used to estimate the excited state vibrational numbering and geometric structures in the combining states. Although the ESR spectrum of BH_2 in a neon matrix has been reported,[4] the microwave and infrared spectra are currently unknown, and, until very recently, the electronic spectrum had not been further explored.

The dearth of electrons has made BH_2 a very attractive candidate for high quality *ab initio* calculations, too numerous to summarize in detail. In early work, Peric *et al.*[5] showed that the original assignments of the bending progression had to be increased by $v' = 2$, so that the observed $^{11}BH_2$ bands are actually 2_0^9–2_0^{13}. There have also been two thorough theoretical studies of the potential energy surfaces and rovibronic term values of the $\widetilde{X}^2A_1$ and $\widetilde{A}^2B_1$ states.[6,7] In both cases, empirical adjustments to the barrier to linearity were made to give better correspondence to the available experimental data. The most recent study,[7] which included the effects of angular momentum and spin-orbit coupling, obtained an adjusted barrier to linearity of 2666 cm^{-1}, ground and excited state r_e structures of $r'' = 1.1875$ Å, $\theta'' = 129.04°$, $r' = 1.1698$ Å, and $\theta' = 180°$, and predicted spin-splittings for both the ground and excited state rovibronic levels.

Very recently,[8] we showed that cold BH_2 radicals could be produced in a discharge jet using a precursor mixture of diborane (B_2H_6) in high pressure argon and detected by laser induced fluorescence.[8] We were able to extend the $^{11}BH_2$ spectrum up to 21 000 cm^{-1}, spanning bending levels from $v_2' = 10$ to 19 along with the detection of a few stretch-bend combination levels for the first time. We also studied the spectrum of $^{11}BD_2$, detecting bands in the bending progression from 2_0^{14} to 2_0^{23} and some stretch-bend combinations. The corresponding ^{10}B isotopologues were also studied. Many of the bands exhibited spin splittings, especially at low N values. Each band was rotationally analyzed and assignments were made for the observed rovibronic lines. The 2_0^{20} band of $^{11}BD_2$ was recorded at high resolution and ground state combination differences formed to refine the lower state rotational constants which led to an improved ground state r_0 structure of BH_2 as $r(BH) = 1.197(2)$ Å, $\theta = 129.6(2)°$.

In conjunction with the experimental work, new very high level hybrid *ab initio* BH_2 potential energy surfaces were generated starting from the coupled cluster singles and doubles with perturbative triples [CCSD(T)]/aug-cc-pV5Z level of theory. The potentials were corrected for core correlation, extrapolation to the complete basis set limit,

a)Author to whom correspondence should be addressed: dclaser@uky.edu.

electron correlation beyond CCSD(T), and diagonal Born-Oppenheimer effects, in order to obtain the highest possible accuracy. These potentials were used in variational calculations of the spin-rovibronic states of the various isotopologues of BH_2 without any empirical adjustments or fitting to experimental data. The agreement with the full range of the new LIF data was excellent, approaching near-spectroscopic accuracy (a few cm^{-1}), and allowed us to understand the complicated spin-rovibronic energy level structure even in the region of strong Renner-Teller resonances.

In the present work, we have used low resolution emission and high resolution stimulated emission pumping (SEP) spectroscopies to elucidate the rovibronic energy levels of $^{11}BH_2$ in the electronic ground state. The molecular constants of the $v = 0$ level have been refined and the spin-rovibrational energies have been determined. The bending levels have been measured from below and up through the barrier to linearity ($v_2'' = 1$–5), showing the details of the reordering of rotational energies in the region of the barrier. The experimental results have been compared with our theoretical predictions of the spin-rovibronic energy levels.

II. EXPERIMENT

The $^{11}BH_2$ free radical was produced in a discharge free jet expansion[9] using precursor mixtures of 0.5%–0.1% diborane (B_2H_6) in high pressure argon, as discussed in more detail elsewhere.[8]

Low-resolution LIF spectra were recorded by exciting the jet-cooled radicals with the collimated beam of a pulsed tunable dye laser (Lumonics HD-500, linewidth 0.1 cm^{-1}) and imaging the resulting fluorescence signals onto the photocathode of a high gain photomultiplier (EMI 9816QB). The signals were sampled with a gated integrator and recorded with LabVIEW-based data acquisition software. The spectra were calibrated with optogalvanic lines from neon- and argon-filled hollow cathode lamps to an accuracy of ~0.1 cm^{-1}. In some cases, the LIF spectra were overlapped by bands of various impurity molecules. To circumvent these problems, we used the LIF synchronous scanning (sync-scan) technique described previously.[10] In this method, the fluorescence is dispersed by a scanning monochromator that is fixed on a prominent emission band of the isotopologue(s) of interest. The excitation laser and the monochromator are scanned synchronously under computer control so that the resulting spectrum exhibits only those transitions that emit down to the chosen level, focusing on the spectrum of a subset of the molecular isotopologues and minimizing impurity emission.

High resolution sync-scan LIF spectra were obtained in the same fashion but using a dye laser equipped with an intracavity angle-tuned etalon (Scanmate 2E), providing tunable radiation with a linewidth of 0.035 cm^{-1}. All high resolution spectra were calibrated with iodine LIF transitions.[11]

Survey low resolution single rotational level emission spectra were obtained by tuning the LIF laser to a single rotational line in the LIF spectrum and focusing the resulting fluorescence with an f1.5 lens system onto the entrance slit of a 0.5 m scanning monochromator (Spex 500M). The pulsed fluorescence signals were detected with a red-sensitive photomultiplier (RCA C31034A), amplified by a factor of 800, sampled with a gated integrator, and recorded digitally. The emission spectra were calibrated to an accuracy of ~2 cm^{-1} using emission lines from an argon discharge lamp. A 1200 line/mm grating blazed at 750 nm was employed in this work, with a bandpass of 0.3–0.6 nm, depending on the strength of the dispersed fluorescence signal.

Stimulated emission pumping (SEP) techniques were employed to measure the ground electronic state rovibronic levels with high precision using the time-gated reference method of Northrup and Sears.[12] The pump laser was the Lumonics HD 500 dye laser (~3–4 mJ/pulse, Coumarin 485, 503, and 540A laser dyes, linewidth ~0.1 cm^{-1}) which was tuned to a single feature in the LIF spectrum, pumping one or two upper state spin-rovibronic energy levels. The dump laser was the Scanmate 2E dye laser operated with the etalon in the cavity (0.5-2 mJ/pulse, various green and red laser dyes, linewidth ~0.035 cm^{-1}) and scanned 2–10 cm^{-1} at a time by angle tuning. It was temporally delayed ca. 100 ns after the pump laser and the two dye laser beams were counter-propagated through the LIF apparatus, crossing at a slight angle in the interaction region. With such a short dump laser delay, the excited target molecules did not travel any appreciable distance downstream, so the pump and dump lasers could be spatially overlapped in the viewing region of the detector.

The fluorescence decay was monitored either as total fluorescence through a long pass or bandpass filter or as a narrow band of emission wavelengths through the monochromator, depending on the wavelength region of interest. The photomultiplier was terminated with a small resistor (50 Ω) so that we could use fast timing to discriminate against the initial discharge flash and scattered laser light and observe the undistorted fluorescence decay profile. When the dump laser was in resonance with the excited state level and a ground state vibrational level, the stimulated emission was detected as a dip in the fluorescence intensity. We found that the best SEP signals were obtained with the first gated integrator (Gate1, 60 ns wide) positioned 20 ns after the pump laser and the second gated integrator (Gate2, 60 ns wide) located 40 ns after the dump laser. Signals from both gates were collected digitally, and the SEP signals displayed as the relative ratio of (Gate2) to (Gate1). The SEP spectra were calibrated by simultaneously recording I_2 LIF signals[11] from a small portion of the residual dump laser beam.

In practice, the SEP signals were wider (0.06–0.08 cm^{-1}) than the dump laser linewidth due to a combination of power broadening and unresolved spin and/or hyperfine structure in the $^{11}BH_2$ lines.

III. THEORETICAL CALCULATIONS

These have been described in detail in our previous work.[8] Briefly, potential energy surfaces of the bent ground $\widetilde{X}^2A_1$ and the linear $\widetilde{A}^2B_1$ first excited states of BH_2 were generated from a series of coupled cluster singles and doubles with perturbative triples [CCSD(T)] level of theory single point calculations with the aug-cc-pV5Z basis set. These surfaces were then

corrected in a systematic fashion for core correlation, complete basis set extrapolation, electron correlation beyond CCSD(T), and diagonal mass dependent Born-Oppenheimer effects.

The corrected *ab initio* surfaces were used without any empirical adjustment for the variational calculation of the ground and excited state energy levels. In previous work, spin-rovibronic calculations for $J \leq 7/2$ were performed, thus enabling the prediction of the energies for all rovibrational levels with $K_a \leq 3$ (Σ, Π, Δ, Φ levels). All four experimentally relevant isotopologues ($^{11}BH_2$, $^{10}BH_2$, $^{11}BD_2$, $^{10}BD_2$) were studied, for energies up to 22 000 cm^{-1} above the $\widetilde{X}^2A_1(000)$ level. We showed that such calculations gave agreement to near-spectroscopic accuracy (a few cm^{-1}) for excited state energy levels as high as (0, 19, 0), some 21 000 cm^{-1} above the ground state zero-point level. In the present work, we extend the computations for $^{11}BH_2$ up to $J = 13/2$ and we compare our high precision SEP measurements of $^{11}BH_2$ ground state spin-rovibronic levels to the calculations up to and above the barrier to linearity.

The ground state molecular structure and rotational, centrifugal distortion, and spin-rotation constants were further explored using the GAUSSIAN 09 suite of programs.[13] This involved a density functional theory (DFT) calculation with the Becke three-parameter hybrid density functional[14] with the Lee, Yang, and Parr correlation (B3LYP) functional[15] and Dunning's correlation consistent basis sets[16] augmented by diffuse functions (aug-cc-pV6Z). Centrifugal distortion and spin-rotation constants were derived from second derivatives of the DFT energies using standard vibrational second order perturbation theory (VPT2)[17] as implemented in the GAUSSIAN code.

IV. EXPERIMENTAL RESULTS AND ANALYSIS

A. Introduction

BH_2 is a bent near-prolate asymmetric top in the ground state and the first electronic transition is $\widetilde{A}^2B_1(\Pi_u)$–$\widetilde{X}^2A_1$, which follows *c*-type rotational selection rules. The presence of two equivalent hydrogen nuclei necessitates a 3:1 [eo, oe: ee,oo] nuclear statistical weight alternation in the populations of the lower state levels of BH_2. We label the energy levels of both states by the asymmetric top quantum numbers N_{KaKc} in the absence of resolvable electron spin splittings. In the upper linear state, K'_a designates the value of l', while the two values of K'_c distinguish the l-type doubling components. In those instances where the spin splittings are resolved, the rotational levels are designated by J, the quantum number for the total rotational plus spin angular momentum: $J = N + 1/2$ (F_1) and $J = N - 1/2$ (F_2). The vibrations of BH_2 are labeled $\nu_1(a_1)$ = BH symmetric stretch, $\nu_2(a_1)$ = bend, and $\nu_3(b_2)$ BH antisymmetric stretch, and vibrational levels are denoted by (ν_1, ν_2, ν_3).

B. LIF spectra and the vibrationless level of the ground state

In their original study of the BH_2 electronic spectrum, Herzberg and Johns[1] used ground state combination differences (GSCDs) and fitting to obtain the ground state $v = 0$ energy levels of $^{11}BH_2$. Unfortunately, due to limitations in the data (only one band in their spectra exhibited any resolvable spin splittings), these levels did not include any spin splittings. In our recent extensive study of the BH_2 LIF spectrum,[8] many of the transitions to higher vibrational levels in the excited state were found to have resolved spin splittings, affording the opportunity to refine the previous results. In the present work, we have recorded the (0,16,0) Π ($K'_a = 1 - K''_a = 0$ and $K'_a = 1 - K''_a = 2$ sub-bands) band and the (0,17,0) Σ ($K'_a = 0 - K''_a = 1$) and Δ ($K'_a = 2 - K''_a = 1$) LIF bands of $^{11}BH_2$ at our highest resolution (observed linewidths ~0.06 cm^{-1}) and derived GSCDs from the data. Examples of the spectra are shown in Fig. 1. Some transitions exhibited obvious spin-splittings and the J quantum numbers were assigned based on relative intensities which scale as the lower state degeneracy of $2J'' + 1$. The observed transitions and their associated assignments are summarized in Tables I and II and include intervals involving $K''_a = 0$, 1, and 2 which can be used to form various GSCDs. In addition, we have measured stimulated emission pumping spectra through the (0,15,0) $^rR_1(1)$ and $^rQ_1(3)$ transitions down to the appropriate ground state $K''_a = 3$ levels. By subtracting the wavenumbers of the SEP transitions from the pump wavenumbers (measured again at high resolution), we obtained GSCDs involving $K''_a = 3$, with spin splittings.

The ground state intervals were fitted to Watson's *A* reduction of the asymmetric top rotational Hamiltonian in the I^r representation involving

$$H_{\text{eff}} = H_R + H_{CD} + H_{SR}.$$

Here, H_R and H_{CD} refer to the rotational energy and its centrifugal distortion corrections and H_{SR} takes into account the interaction of the spin of the unpaired electron and the molecular rotation. The rotational constants A, B, and C were varied along with the quartic centrifugal distortion constants and the major spin constant ε_{aa}. The resulting constants are presented in Table III along with the constants we obtained

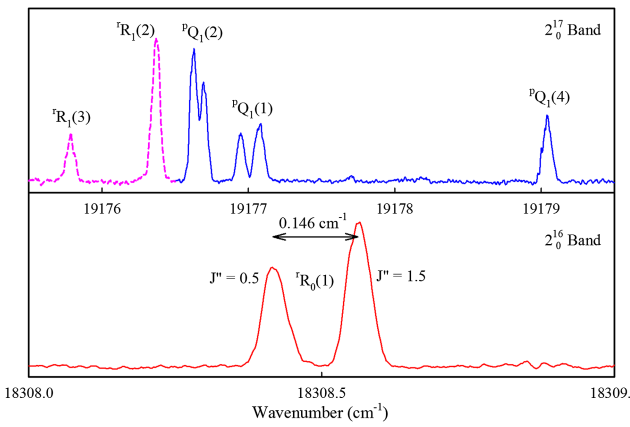

FIG. 1. Examples of the high-resolution LIF spectra of $^{11}BH_2$ recorded in this work. The top panel shows part of the Q-branch of the 2^{17}_0 Σ band, with resolved spin-splittings for the first two members of the branch. The dashed segment of the top panel is a portion of the corresponding Δ band. The bottom panel shows the two spin-components of the $^rR_0(1)$ transition of the $2^{16}_0\Pi$ band, with a measured spin splitting of 0.146 cm^{-1}. The lower state J quantum numbers were assigned based on the relative intensities of the two lines.

TABLE I. The high-resolution LIF spectrum of the 2_0^{16} band of $^{11}BH_2$.

Branch	N', Ka', Kc', J'	N'', Ka'', Kc'', J''	Transition (cm^{-1})	Spin splitting (cm^{-1})
$^rR_0(0)$[a]	1, 1, 0, 0.5	0, 0, 0, 0.5	18 295.359 0	
	1, 1, 0, 1.5	0, 0, 0, 0.5	18 295.661 7	0.3027
$^rR_0(1)$	2, 1, 1, 1.5	1, 0, 1, 0.5	18 308.416 4	
	2, 1, 1, 2.5	1, 0, 1, 1.5	18 308.562 4	0.1460
$^rR_0(2)$	3, 1, 2, 2.5	2, 0, 2, 1.5	18 321.925 8	
	3, 1, 2, 3.5	2, 0, 2, 2.5	18 322.013 6	0.0878
$^rR_0(3)$	4, 1, 3, 3.5	3, 0, 3, 2.5	18 336.199 4	
	4, 1, 3, 4.5	3, 0, 3, 3.5	18 336.268 8	0.0694
$^rR_0(4)$	5, 1, 4, 4.5	4, 0, 4, 3.5	18 351.483 8	
	5, 1, 4, 5.5	4, 0, 4, 4.5	18 351.533 5	0.0497
$^rR_0(5)$	6, 1, 5	5, 0, 5	18 368.541 7	
$^rQ_0(1)$	1, 1, 1, 0.5	1, 0, 1, 0.5	18 281.044 3	
	1, 1, 1, 1.5	1, 0, 1, 1.5	18 281.402 9	0.3586
$^rQ_0(3)$	3, 1, 3, 2.5	3, 0, 3, 2.5	18 269.444 4	
	3, 1, 3, 3.5	3, 0, 3, 3.5	18 269.536 4	0.0920
$^rQ_0(4)$	4, 1, 4, 3.5	4,0, 4, 3.5	18 263.865 8	
	4, 1, 4, 4.5	4,0, 4, 4.5	18 263.951 6	0.0858
$^rQ_0(5)$	5, 1, 5, 4.5	5, 0, 5, 4.5	18 259.144 7	
	5, 1, 5, 5.5	5, 0, 5, 5.5	18 259.281 6	0.1369
$^rP_0(2)$	1, 1, 0, 0.5	2, 0, 2, 1.5	18 255.667 3	
	1, 1, 0, 1.5	2, 0, 2, 2.5	18 255.972 4	0.3051
$^rP_0(3)$	2, 1, 1, 1.5	3, 0, 3, 2.5	18 242.400 5	
	2, 1, 1, 2.5	3, 0, 3, 3.5	18 242.551 7	0.1512
$^rP_0(4)$	3, 1, 2, 2.5	4, 0, 4, 3.5	18 229.780 6	
	3, 1, 2, 3.5	4, 0, 4, 4.5	18 229.869 1	0.0885
$^rP_0(5)$	4, 1, 3, 3.5	5, 0, 5, 4.5	18 218.198 3	
	4, 1, 3, 4.5	5, 0, 5, 5.5	18 218.255 6	0.0573
$^rP_0(6)$	5, 1, 4	6, 0, 6	18 207.970 1	
$^rP_0(7)$	6, 1, 5	7, 0, 7	18 199.803 7	
$^pR_2(2)$	3, 1, 3, 3.5	2, 2, 1, 2.5	18 173.251 5	
	3, 1, 3, 2.5	2, 2, 1, 1.5	18 173.432 0	0.1805
$^pR_2(3)$	4, 1, 4, 4.5	3, 2, 2, 3.5	18 180.461 0	
	4, 1, 4, 3.5	3, 2, 2, 2.5	18 180.541 2	0.0802
$^pR_2(3)$	4, 1, 3, 4.5	3, 2, 1, 3.5	18 200.0025	
	4, 1, 3, 3.5	3, 2, 1, 2.5	18 200.130 8	0.1283
$^pR_2(4)$	5, 1, 5, 4.5	4, 2, 3, 3.5	18 188.196 3	
	5, 1, 5, 5.5	4, 2, 3, 4.5	18 188.165 9	0.0304
$^pQ_2(2)$	2, 1, 1, 2.5	2, 2, 1, 2.5	18 146.240 8	
	2, 1, 1, 1.5	2, 2, 1, 1.5	18 146.353 4	0.1126
$^pQ_2(3)$	3, 1, 3, 3.5	3, 2, 1, 3.5	18 133.281 3	
	3, 1, 3, 2.5	3, 2, 1, 2.5	18 133.375 4	0.0642
$^pQ_2(4)$	4, 1, 3, 4.5	4, 2, 3, 4.5	18 147.147 9	
	4, 1, 3, 3.5	4, 2, 3, 3.5	18 147.216 6	0.0537
$^pQ_2(5)$	5, 1, 5	5, 2, 3	18 120.863 4	
$^pP_2(2)$	1, 1, 1, 0.5	2, 2, 1, 1.5	18 118.990 1	
	1, 1, 1, 1.5	2, 2, 1, 2.5	18 119.074 9	0.0848
$^pP_2(3)$	2, 1, 1	3, 2, 1	18 106.285 0	
$^pP_2(4)$	3, 1, 3	4, 2, 3	18 080.459 9	
$^pP_2(5)$	4, 1, 3	5, 2, 3	18 079.888 5	

[a]Transitions without J quantum numbers did not have resolvable spin-splittings.

from our B3LYP/aug-cc-pV6Z theoretical study and by fitting the energy levels obtained from our *ab initio* potential energy surface calculations. Finally, we also fitted the energy levels reported by Herzberg and Johns[1] (which extend to much higher N and K_a but do not involve any spin splittings) to the same Hamiltonian with the spin constants constrained to 0.0, and these results are also presented in Table III. It is clearly evident that there is generally good agreement between the various sets of constants.

Using our experimentally derived constants, we have calculated the ground vibrational state energy levels of $^{11}BH_2$ up to $K_a''=2$, $N''=5$, which is the range covered by our SEP data for higher vibrational levels. These are summarized in Table IV where they are also compared to our theoretical predictions.

C. Emission spectra

Some typical single rotational level emission spectra of $^{11}BH_2$ are shown in Fig. 2. The top panel shows the spectrum obtained after broadband (0.1 cm^{-1}) laser pumping of the two spin-components of the $^rR_0(1)$ transition of the $2_0^{16}\Pi$ band (see Fig. 1). The upper state $N=2$, $K_a=1$, $K_c=1$ level emits down to the $1_{0,1}$, $3_{0,3}$, $2_{2,1}$, and $3_{2,1}$ quartets of rotational states in each ground state bending vibrational level. Weak transitions down to the 1_12_1 and 1_12_2 combination levels are also observed.

The bottom panel shows the emission transitions observed after laser pumping of the $^rQ_1(2)$ transition of the 2_0^{17} Δ band. The upper state $2_{2,0}$ level emits down to the $K_a=1$, $N=1,2,3$ levels in a single unresolved feature and down to the $3_{3,0}$ level at higher energy. If the rotational levels follow the typical asymmetric top pattern, as they do for the (0,0,0) state, then the $K_a=1$ lines in the lower panel should lie between the $1_{0,1}$ and $3_{3,0}$ features in the top panel. The vertical dotted leaders show the expected position at the top end and the observed position at the bottom end. It is readily apparent that the usual pattern is found for the (0,1,0) and (0,2,0) levels but that the $K_a=1$ levels fall progressively further below $K_a=0$ for $v_2=3$–5. Two other observed trends are that the separation of the outer members of the quartets increase from (0,1,0) to (0,3,0) and then decrease for (0,4,0) and that the $K_a=3-K_a=0$ intervals increase from $v_2=1$ to 3 and then level off at $v_2=4$. As will be explored more fully in Sec. V, all of these trends are as expected for levels near and above the barrier to linearity as the molecule transitions from a bent to a linear geometry.

TABLE II. The high resolution LIF spectrum of the $2_0^{17}\Sigma$ and Δ LIF bands of $^{11}BH_2$.

Band	Branch	N', K_a', K_c', J'	N'', K_a'', K_c'', J''	Transition (cm^{-1})	Spin splitting (cm^{-1})
(0,17,0)Σ	$^pR_1(1)$[a]	2,0,2,2.5	1,1,0,1.5	19 200.643 6	
		2,0,2,1.5	1,1,0,0.5	19 200.781 4	0.1378
	$^pR_1(2)$	3,0,3,3.5	2,1,1,2.5	19 211.209 0	
		3,0,3,2.5	2,1,1,1.5	19 211.285 1	0.0761
	$^pR_1(3)$	4,0,4,4.5	3,1,2,3.5	19 222.067 0	
		4,0,4,3.5	3,1,2,2.5	19 222.117 4	0.0504
	$^pR_1(4)$	5,0,5	4,1,3	19 233.757 9	
	$^pR_1(5)$	6,0,6	5,1,4	19 246.463 8	
	$^pQ_1(1)$	1,0,1,1.5	1,1,1,1.5	19 176.948 9	
		1,0,1,0.5	1,1,1,0.5	19 177.078 3	0.1294
	$^pQ_1(2)$	2,0,2,2.5	2,1,2,2.5	19 176.625 8	
		2,0,2,2.5	2,1,2,2.5	19 176.696 5	0.0707
	$^pQ_1(3)$	3,0,3	3,1,3	~19 177.04[b]	
	$^pQ_1(4)$	4,0,4	4,1,4	19 179.043 4	
	$^pP_1(1)$	0,0,0,0.5	1,1,0,1.5	19 163.439 1	
		0,0,0,0.5	1,1,0,0.5	19 163.566 7	0.1276
	$^pP_1(2)$	1,0,1,1.5	2,1,1,2.5	19 148.000 3	
		1,0,1,0.5	2,1,1,1.5	19 148.063 4	0.0631
	$^pP_1(3)$	2,0,2	3,1,2	19 131.394 5	
	$^pP_1(4)$	3,0,3	4,1,3	19 114.361 4	
	$^pP_1(5)$	4,0,4	5,1,4	19 097.742 0	
(0,17,0)Δ	$^rR_1(1)$	2,2,0	1,1,0	19 162.922 3	
	$^rR_1(1)$	2,2,1	1,1,1	19 164.541 3	
	$^rR_1(2)$	3,2,1,2.5	2,1,1,1.5	19 170.812 2	
		3,2,1,3.5	2,1,1,2.5	19 170.837 8	0.0256
	$^rR_1(2)$	3,2,2	2,1,2	19 176.372 5	
	$^rR_1(3)$	4,2,2	3,1,2	19 175.784 1	
	$^rR_1(3)$	4,2,3	3,1,3	19 188.419 4	
	$^rQ_1(2)$	2,2,0,1.5	2,1,2,1.5	19 138.836 6	
		2,2,0,2.5	2,1,2,2.5	19 138.895 2	0.0586
	$^rQ_1(2)$	2,2,1	2,1,1	19 135.578 6	
	$^rQ_1(3)$	3,2,2	3,1,2	19 131.106 0	
	$^rQ_1(3)$	3,2,1,2.5	3,1,3,2.5	19 136.635 9	
		3,2,1,3.5	3,1,3,3.5	19 136.675 5	0.0396
	$^rQ_1(4)$	4,2,3	4,1,3	19 125.703 9	
	$^rQ_1(4)$	4,2,2	4,1,4	19 132.743 2	

[a]Transitions without J quantum numbers did not have resolvable spin-splittings.
[b]Overlaps $^pQ_1(1)$.

D. SEP spectra

In order to make more precise measurements of the various spin rovibrational levels indicated in Fig. 2, we resorted to stimulated emission pumping (SEP) spectroscopy, which has superior resolution and wavenumber accuracy (±0.05 cm^{-1}) over our low resolution emission spectra (±1–2 cm^{-1}). Figure 3 shows the various experiments necessary for obtaining the ground state energy levels and indicates the quality of the data in each case. First, a high resolution LIF scan was

TABLE III. The effective ground state (v = 0) molecular constants (in cm^{-1}) of $^{11}BH_2$.

Constant	Expt.[a]	B3LYP/aug-cc-pV6Z	*Ab initio* theory[b]	Previous expt.[c]
A	41.627 2(20)[d]	38.9694	41.5430(66)	41.656(16)
B	7.244 66(254)	7.2759	7.2541(105)	7.2609(72)
C	6.000 83(262)	6.1312	5.9991(103)	5.9860(69)
Δ_K	0.293 27(19)	0.2124	0.2864(11)	0.2967(21)
Δ_{NK}	$-6.02(12) \times 10^{-3}$	-4.6×10^{-3}	$-5.13(45) \times 10^{-3}$	$-5.69(111) \times 10^{-3}$
Δ_N	$3.09(15) \times 10^{-4}$	3.03×10^{-4}	$2.99(71) \times 10^{-4}$	$2.96(33) \times 10^{-4}$
δ_K	$2.42(122) \times 10^{-3}$	9.7×10^{-4}	$3.78(49) \times 10^{-3}$	$7.74(280) \times 10^{-3}$
δ_N	$7.0(15) \times 10^{-5}$	8.2×10^{-5}	$8.7(65) \times 10^{-5}$	$1.28(16) \times 10^{-4}$
H_K	4.044×10^{-3}	...	$3.758(53) \times 10^{-3}$	$4.044(58) \times 10^{-3}$
H_{NK}	-3.12×10^{-5}	...	$-8.6(26) \times 10^{-5}$	$-3.12(168) \times 10^{-5}$
ε_{aa}	0.1481(38)	0.1538	0.1549(57)	...
ε_{bb}	...	0.0013	...	...
ε_{cc}	...	–0.0023	...	...
No. of data points	71	...	58	49
Std. deviation	0.014 cm^{-1}	...	0.03 cm^{-1}	0.10 cm^{-1}

[a]From fitting combination differences measured in this work.
[b]From fitting the rotational energy levels up to $J = 4.5$ and $K_a = 4$ obtained from the *ab initio* potential energy surface.[8]
[c]From fitting the energy levels given in Ref. 1.
[d]The numbers in parentheses are standard errors of 1σ. Constants without errors were fixed in the least squares fitting.

required to identify and accurately measure the wavenumber of the pump transition. In this case, the LIF spectrum is of the two spin-split components of the $^rQ_0(1)$ line of the 2_0^{16} band at about 18 281 cm^{-1} (see bottom inset). Pumping the most intense feature involves the $1_{1,1}$ J′ = 1.5 − $1_{0,1}$ J″ = 1.5 transition at 18 281.402 9 cm^{-1}, which gave the emission spectrum partially shown in Fig. 3, illustrating the strong transitions down to the $1_{0,1}$ and $2_{2,1}$ rotational levels of the $v_2'' = 2$, 3, and

TABLE IV. The observed (upper value from SEP measurements) and calculated (lower value from *ab initio* potential) spin rovibronic energy levels (in cm^{-1}) for the ground state bending vibrational levels of $^{11}BH_2$.

Assignment	Vibrational level[a]					
N, K_a, Kc, J	(0,0,0)[b]	(0,1,0)	(0,2,0)	(0,3,0)	(0,4,0)	(0,5,0)
			$K_a = 0$ levels[c]			
0,0,0	0.000	973.531	1912.489	2859.452	3868.252	...
	0.000	972.869	1910.890	2857.405	3866.207	4951.134
Obs-calc	...	0.662	1.599	2.047	2.045	...
1,0,1	13.244	986.706	1925.612	2872.628	3881.525	...
	13.254	986.061	1924.041	2870.587	3879.481	4964.501
Obs-calc	–0.010	0.645	1.571	2.041	2.044	...
2,0,2	39.692	1013.045	1951.875	2898.946	...	...
	39.720	1012.412	1950.316	2896.923	3905.972	4991.002
Obs-calc	–0.028	0.633	1.559	2.023	...	...
3,0,3	79.264	1052.599	1991.193	2938.347	3947.553	...
	79.319	1051.854	1989.660	2936.354	3945.569	5030.184
Obs-calc	–0.055	0.745	1.533	1.993	1.984	...
4,0,4	131.841	1104.856	2043.499	2990.752	4000.050	...
	131.933	1104.295	2041.996	2988.800	3998.108	5081.462
Obs-calc	–0.092	0.561	1.503	1.952	1.942	...
5,0,5	197.273	1170.142	2108.706	3056.084	4065.288	...
	197.412	1169.606	2107.216	3054.141	4063.344	5156.418
Obs-calc	–0.139	0.536	1.490	1.943	1.944	...

TABLE IV. (*Continued.*)

Assignment	Vibrational level[a]					
N, K_a, Kc, J	(0,0,0)[b]	(0,1,0)	(0,2,0)	(0,3,0)	(0,4,0)	(0,5,0)
			$K_a = 1$ levels			
1,1,1 J = 0.5	47.281	1032.676	…	…	3471.465	…
	47.178	1031.772	1956.416	2741.516	3467.983	4399.208
Obs-calc	0.103	0.904	…	…	3.482	…
1,1,1 J = 1.5	47.392	1033.032	1960.412	…	3473.055	…
	47.308	1032.096	1957.477	2744.096	3469.390	4399.329
Obs-calc	0.084	0.936	2.935	…	3.665	…
1,1,0 J = 0.5	48.514	…	1960.527	…	…	4402.833
	48.417	1033.077	1957.700	2742.607	3469.363	4400.921
Obs-calc	0.097	…	2.827	…	…	1.912
1,1,0 J = 1.5	48.625	…	1961.676	…	…	4402.916
	48.547	1033.400	1958.760	2745.171	3470.760	4401.042
Obs-calc	0.078	…	2.916	…	…	1.874
2,1,2 J = 1.5	72.590	1057.885	1984.549	2772.755	3496.649	4425.699
	72.505	1056.978	1981.687	2767.189	3493.142	4423.854
Obs-calc	0.085	0.907	2.862	5.566	3.507	1.845
2,1,2 J = 2.5	72.651	1058.057	1985.153	2774.172	3497.468	4425.757
	72.577	1057.156	1982.257	2768.499	3493.889	4423.921
Obs-calc	0.074	0.901	2.896	5.673	3.579	1.836
2,1,1 J = 1.5	76.287	1061.807	1988.392	2775.986	3500.763	4430.854
	76.218	1060.888	1985.531	2770.443	3497.270	4428.984
Obs-calc	0.069	0.919	2.861	5.543	3.493	1.870
2,1,1 J = 2.5	76.349	1061.991	1989.003	2777.425	3501.597	4431.002
	76.291	1061.066	1986.105	2771.753	3498.010	4429.053
Obs-calc	0.058	0.925	2.898	5.672	3.587	1.949
3,1,3 J = 2.5	110.474	1095.494	2021.989	2810.040	3533.569	…
	110.411	1094.631	2019.131	2804.479	3530.029	4460.698
Obs-calc	0.063	0.863	2.858	5.561	3.540	…
3,1,3 J = 3.5	110.517	1095.607	2022.399	2811.036	3534.115	…
	110.467	1094.759	2019.530	2805.385	3530.718	4460.763
Obs-calc	0.050	0.848	2.869	5.651	3.397	…
3,1,2 J = 2.5	117.858	1103.294	2029.643	2816.544	3541.710	4472.702
	117.825	1102.436	2026.806	2810.988	3538.212	4470.928
Obs-calc	0.033	0.858	2.837	5.556	3.498	1.774
3,1,2 J = 3.5	117.901	1103.418	2030.065	2817.509	3542.287	4472.786
	117.882	1102.565	2027.210	2811.897	3538.945	4470.996
Obs-calc	0.019	0.853	2.855	5.612	3.342	1.790
4,1,4 J = 3.5	160.910	1145.605	2071.772	2859.547	3582.342	4511.529
	160.872	1144.758	2068.928	2853.957	3578.805	4509.676
Obs-calc	0.038	0.847	2.844	5.590	3.537	1.853

TABLE IV. (*Continued.*)

Assignment	Vibrational level[a]					
N, K_a, Kc, J	(0,0,0)[b]	(0,1,0)	(0,2,0)	(0,3,0)	(0,4,0)	(0,5,0)
4,1,4, J = 4.5	160.943	1145.709	2072.088	2860.302	3582.760	…
	160.945	1144.874	2069.239	2854.637	3579.695	4509.861
Obs-calc	–0.002	0.835	2.849	5.665	3.065	…
4,1,3 J = 3.5	173.191	…	2084.497	…	…	4528.438
	173.198	1157.736	2081.688	2864.789	3592.051	4526.646
Obs-calc	–0.007	…	2.809	…	…	1.792
4,1,3 J = 4.5	173.224	…	2084.830	…	…	…
	173.273	1157.5853	2082.004	2865.472	3593.344	4526.851
Obs-calc	–0.049	…	2.826	…	…	…
5,1,5, J = 4.5	223.845	…	…	…	…	…
	223.827	1207.334	2131.077	2915.513	3642.431	4570.627
Obs-calc	0.018	…	…	…	…	…
5,1,5 J = 5.5	223.872	…	…	…	…	…
	223.950	1207.430	2131.347	2916.300	3640.477	4571.237
Obs-calc	–0.078	…	…	…	…	…
5,1,4 J = 4.5	242.215	1227.483	2152.923	2937.423	…	4597.726
	242.247	1226.739	2150.148	2932.325	3660.793	4595.838
Obs-calc	–0.032	0.744	2.775	5.098	…	1.888
5,1,4 J = 5.5	242.242	1227.587	2153.194	2938.039	…	…
	242.385	1226.839	2150.424	2932.505	3660.657	4596.603
Obs-calc	–0.143	0.748	2.770	5.534	…	…
			K_a = 2 levels			
2,2,1 J = 1.5	175.301	1199.482	2195.849	3151.206	4077.106	…
	175.027	1198.222	2192.476	3145.488	4071.143	5043.861
Obs-calc	0.274	1.260	3.353	5.718	5.963	…
2,2,1, J = 2.5	175.548	1200.025	2197.036	3153.368	4079.375	…
	175.289	1198.747	2193.590	3147.461	4073.129	5044.184
Obs-calc	0.259	1.278	3.446	5.907	6.246	…
2,2,0, J = 1.5	175.334	…	2195.727	…	4077.153	…
	175.060	1198.249	2192.495	3145.466	4071.092	5043.632
Obs-calc	0.274	…	3.232	…	6.061	…
2,2,0, J = 2.5	175.581	…	2196.904	3153.395	4079.413	…
	175.322	1198.772	2193.609	3147.483	4073.178	5044.410
Obs-calc	0.259	…	3.295	5.912	6.235	…
3,2,2 J = 2.5	215.185	…	2235.525	3191.051	4116.997	…
	214.930	1238.064	2232.304	3185.312	4110.963	5083.439
Obs-calc	0.255	…	3.221	5.739	6.034	…
3,2,2 J = 3.5	215.357	…	2236.334	3192.561	4118.540	…
	215.113	1238.436	2233.091	3186.686	4112.365	5083.812
Obs-calc	0.244	…	3.243	5.875	6.175	…

TABLE IV. (*Continued.*)

Assignment	Vibrational level[a]					
N, K_a, Kc, J	(0,0,0)[b]	(0,1,0)	(0,2,0)	(0,3,0)	(0,4,0)	(0,5,0)
3,2,1 J = 2.5	215.350	...	2235.598	3191.174	4117.234	...
	215.094	1238.189	2232.399	3185.421	4111.212	5084.567
Obs-calc	0.256	...	3.199	5.753	6.021	...
3,2,1 J = 3.5	215.522	...	2236.431	3192.654	4118.767	...
	215.277	1238.561	2233.185	3186.794	4112.612	5084.927
Obs-calc	0.245	...	3.246	5.860	6.155	
4,2,3 J = 3.5	268.248	1292.271	2288.401	...	...	...
	268.025	1291.049	2285.176	3238.070	4163.829	5133.014
Obs-calc	0.223	1.222	3.225	...	...	...
4,2,3 J = 4.5	268.381	1292.558	2289.017	3244.971	4171.027	...
	268.177	1291.347	2285.782	3239.194	4164.945	5134.024
Obs-calc	0.204	1.211	3.235	5.777	6.082	...
4,2,2 J = 3.5	268.738	...	2288.658	...	...	...
	268.514	1291.427	2285.458	3238.396	4164.574	5134.501
Obs-calc	0.224	...	3.200	...	...	...
4,2,2 J = 4.5	268.871	1292.907	2289.278	3245.263	4171.708	...
	268.666	1291.719	2286.063	3239.519	4165.680	5136.587
Obs-calc	0.205	1.188	3.215	5.744	6.028	...
5,2,3 J = 4.5	335.576	1359.256	2354.879	3310.363	4237.587	...
	335.411	1358.020	2351.780	3304.642	4231.617	
Obs-calc	0.165	1.236	3.099	5.721	5.970	...
5,2,3 J = 5.5	335.683	1359.426	2355.466	3311.266	4238.473	...
	335.558	1358.303	2352.338	3305.540	4232.533	
Obs-calc	0.125	1.123	3.128	5.726	5.940	...
5,2,4 J = 4.5	334.444	...	...	...	...	...
	334.282	1357.158	2351.127	3303.886	4229.898	
Obs-calc	0.162	...	...	...	...	...
5,2,4 J = 5.5	334.552	...	...	...	...	...
	334.430	1357.4433	2351.6879	3304.7900	4230.8302	
Obs-calc	0.122	...	...	...	...	...

[a]For each set of quantum numbers, the first entry is the observed value (where available), with the calculated value directly below it. Observed values have an estimated uncertainty of ±0.05 cm^{-1}. The following $K_a = 3$ levels were also observed: (0,1,0): 3,3,1, J = 2.5: (0,1,0) = 1447.837, obs-calc = 2.153 cm^{-1}; (0,2,0) = 2512.995 cm^{-1}, obs-calc = 3.487 cm^{-1}. 3,3,1, J = 3.5 (0,1,0) = 1448.597 cm^{-1}, obs-calc = 2.152 cm^{-1}.

[b]The (0,0,0) observed levels were calculated from the experimental constants in Table III. They have an estimated uncertainty of ±0.03 cm^{-1}.

[c]The $K_a = 0$ levels do not have any appreciable spin-splittings.

4 bending states. Once the emission lines were approximately measured, the high-resolution dump laser was slowly scanned through the appropriate region and the SEP spectrum recorded along with I_2 LIF calibration data. The top panels in Fig. 3 show typical SEP data. The left-hand inset shows the transition from the pumped level dumped down to the two spin-components ($2_{2,1}$ $J = 1.5$ and 2.5) of the (0,3,0) vibrational state, with a spin-splitting of 2.16 cm^{-1}, in good agreement with our *ab initio* calculated splitting of 1.97 cm^{-1}. The center inset shows a similar measurement for the (0,2,0) state, with a spin-splitting of 1.18 cm^{-1}, comparable to the calculated value of 1.11 cm^{-1}. The right-hand inset shows the SEP spectrum of the transition to the $1_{0,1}$ $J = 0.5$ and 1.5 levels, which appears as a single line since there are no appreciable spin-splittings

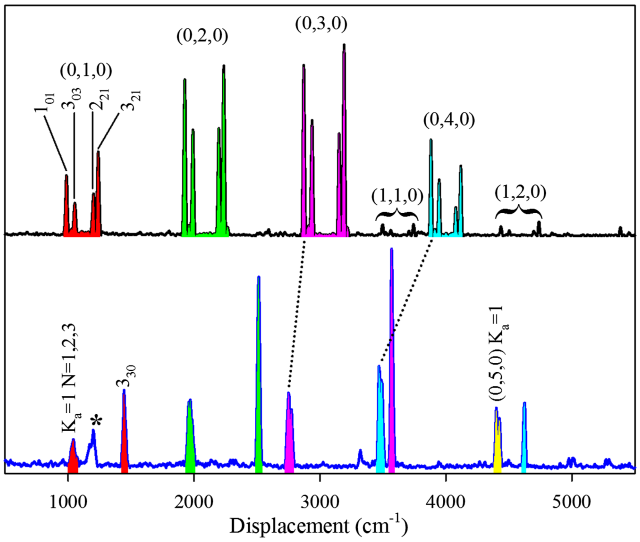

FIG. 2. Typical $^{11}BH_2$ single rotational level emission spectra. In each case, the wavenumber scale is displacement from the laser wavenumber, which gives a direct measure of the relative ground state energy for each transition. The top panel shows the spectrum obtained after broadband (0.1 cm^{-1}) laser pumping of the two spin-components of the $^rR_0(1)$ transition of the $2_0^{16}\Pi$ band (see Fig. 1). The upper state $N=2$, $K_a=1$, $K_c=1$ level emits down to the $1_{0,1}$, $3_{0,3}$, $2_{2,1}$, and $3_{2,1}$ quartets of rotational states in each ground state bending vibrational level. Weak transitions down to the 1_12_1 and 1_12_2 combination levels are also observed. The bottom panel shows the emission transitions observed after laser pumping of the $^rQ_1(2)$ transition of the 2_0^{17} Δ band. The upper state $2_{2,0}$ level emits down to the $K_a=1$, $N=1,2,3$ levels in a single unresolved feature and down to the $3_{3,0}$ level at higher energy. The asterisk indicates an impurity transition. The top ends of the dotted lines show the expected position of the $K_a=1$ levels in the absence of reordering, and the bottom ends show the actual observed position for each vibrational level.

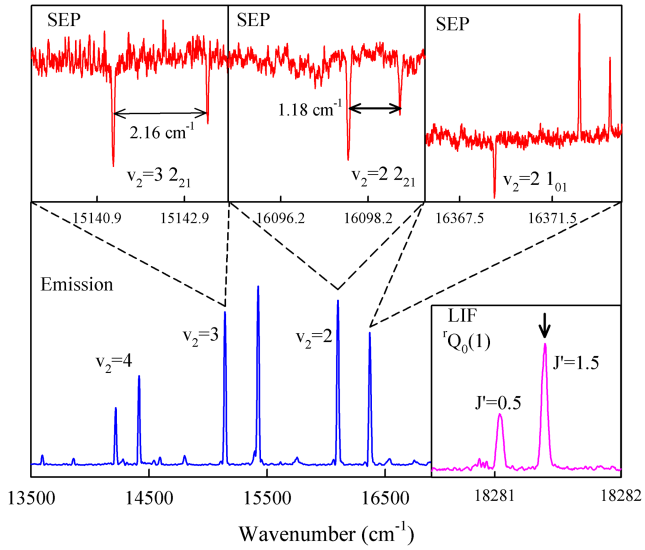

FIG. 3. Example Stimulated Emission Pumping (SEP) spectra. The inset at the bottom right shows a small segment of the 2_0^{16} high resolution LIF spectrum. The arrow indicates the $J'=1.5$ $^rQ_0(1)$ transition pumped by the laser to obtain the emission spectrum shown at the bottom of the figure. Each observed emission band consists of two strong features down to the $1_{0,1}$ and $2_{2,1}$ rotational states of a ground state bending level. The upper panels show the corresponding SEP spectra with observed spin-splittings for the $2_{2,1}$ levels. The positive going transitions in the right most SEP panel are extraneous LIF transitions excited by the dump laser.

in the $K_a=0$ rotational levels. The scan also shows two extraneous features due to direct LIF features excited by the dump laser, a complication in some of the spectra. By laboriously working our way through the emission spectra of ten individual LIF transitions involving the 2_0^{16} and 2_0^{17} bands and taking advantage of the selection rules for transitions from the Σ, Π, and a few Δ levels, we were able to map out a large number of ground state spin rotation-vibration levels. Since this necessitated many dye changes for the dump laser and slow etalon scans with considerable signal averaging, acquisition of the spectra involved the work of most of a year.

The derivation of the final ground state energy levels from the SEP spectra involved the following calculation: E (v, J, K_a, K_c) = Pump transition (cm^{-1} ± 0.005 cm^{-1}) – SEP transition (cm^{-1} ± 0.04 cm^{-1}) + Ground state energy of pump transition (cm^{-1} ± 0.03 cm^{-1}). Propagation of error indicates that the final energy values have an associated uncertainty of ±0.05 cm^{-1}, which is our estimated accuracy of these measurements. The results are given in Table IV, which summarizes in compact form the experimental measurements and the corresponding theoretically calculated energy levels from $v_2=0$ to 5. Various experimental and/or signal-to-noise considerations limited our ability to measure all of the energy levels, accounting for the gaps in the table. We were only able to measure a very few levels involving the (0,5,0) state due to the weakness of the emission transitions to this high bending level of the ground state.

V. DISCUSSION

A. Comparison between theory and experiment

Our measured bending levels occur at 973.53, 1912.49, 2859.45, and 3868.25 cm^{-1} ($v_2=1$–4, $0_{0,0}$). These values are all very slightly higher than our theoretical predictions,[8] which have a maximum error of 2.05 cm^{-1} (0.05%) for $v_2=4$ (see Table IV). Previously reported vibronic term values for the (0,4,0) state from empirically adjusted *ab initio* potentials are 3888 cm^{-1} (Ref. 6) and 3880.6 cm^{-1} (Ref. 7), both somewhat higher than our SEP value.

From our low resolution emission spectra, we can obtain an approximate value of the ν_1 stretching fundamental (~2509 cm^{-1}) which compares favorably with our theoretical value of 2508.1 cm^{-1} and previous values[6,7] of 2518 and 2506.5 cm^{-1}. In a similar fashion, we estimate the (1,1,0) and (1,2,0) vibronic term values from the emission spectra at ~3482 and ~4423 cm^{-1}, compared with our theoretical values[8] of 3482.1 and 4421.9 cm^{-1}.

Consideration of the results in Table IV shows that for the lowest vibrational level, the agreement between observed and calculated rotational levels is very good, with a maximum deviation of 0.28 cm^{-1}, which occurs in the $K_a=2$ manifold. Where there are significant spin splittings ($K_a=1$ and 2), the obs-calc residuals are very similar for both J values, indicating that the effects of the unpaired electron spin are reasonably well modeled by the theory. This conclusion is buttressed by the fitted experimental and *ab initio* spin constants ε_{aa} (Table III) that overlap each other within their standard deviations.

Turning to the higher bending levels, it is immediately apparent that the experimental values are always greater than

the theoretical ("calculated" in Table IV) values and that the residuals are fairly consistent within a given K_a stack of any particular vibrational level. For example, for (0,1,0), the residuals are ~0.6 cm^{-1} for $K_a = 0$, ~0.8 cm^{-1} for $K_a = 1$, and ~1.2 cm^{-1} for $K_a = 2$. For (0,4,0), the residuals for those same K_a stacks are ~2.0 cm^{-1}, ~3.5 cm^{-1}, and ~6.0 cm^{-1}. The regularity of the residuals lends credence to our assignments of the SEP spectra. In our initial analysis of the SEP data, a small number of misassignments were immediately obvious as they broke the expected pattern of residuals and were easily identified.

B. Reordering of levels near the barrier to linearity

In our previous work,[8] we obtained the energy difference (or barrier to linearity) between the energy minima of the analytical potential energy surfaces of $^{11}BH_2$ without the mass dependent corrections as 2655.7 cm^{-1}. Since our emission and SEP data samples ground state rovibronic bending levels from 0.0 up to a maximum of 4597.7 cm^{-1} [(0,5,0) J = 5.5, $5_{1,4}$], the measurements straddle the regions below, through, and above the barrier. This can be easily seen by an examination of the low resolution emission data in Fig. 2 and more clearly from the measured rotational levels in Table IV. For the first bending level (0,1,0 = 973.5 cm^{-1}), the rotational states follow the classic prolate asymmetric top order with $1_{0,1} < 1_{1,0} < 2_{2,1} < 3_{3,0}$. The pattern is similar for $\nu_2 = 2$ (0,2,0 = 1912.5 cm^{-1}) although the difference between $1_{0,1}$ and $1_{1,0}$ has *decreased* from 46.3 cm^{-1} in (0,1,0) to 34.9 cm^{-1} in (0,2,0), rather than the expected increase as the bond angle opens and A_{eff} increases. This is the first sign of a phenomenon called K-reordering in which A_{eff} decreases with increasing vibrational excitation. The third bending level (0,3,0 = 2859.5 cm^{-1}) is expected to be slightly above the barrier, and it is immediately obvious from the data in Fig. 2 and Table IV that reordering has occurred with $1_{1,0} < 1_{0,1}$. Now $1_{0,1} - 1_{1,0} = -129$ cm^{-1} and A_{eff} is now substantially negative.

We find reordering to be a subtle and conceptually difficult concept, so here we review some of the relevant aspects from the literature. We start with the effects of quasi-linearity in bent molecules as discussed by Johns[18] some 50 years ago. As a nonlinear asymmetric top molecule in a nondegenerate electronic state bends towards linearity, one might naively expect that the value of the A_{eff} rotational constant (essentially the interval between the $K_a = 0$ and $K_a = 1$ levels) would tend towards infinity. In fact, a correlation of the energy levels of the molecule in the bent and linear forms shows that A_{eff} becomes the bending frequency of the linear molecule. As first described by Dixon,[19] successive vibrational intervals in the bending progression of a quasi-linear molecule with no electronic orbital angular momentum ($\Lambda = 0$) have a minimum in the region of the potential barrier.

If the bent/linear pair are in electronic states with nonzero orbital angular momentum ($\Lambda > 0$), then the situation is markedly more complex as angular momentum coupling [the Renner-Teller (RT) effect] has to be taken into account. As originally discovered by Merer and co-workers,[20–22] some of the rovibronic energy levels of the lower Renner-Teller component undergo a rearrangement from the usual pattern near the barrier to linearity. This is what is termed "reordering" and is one of the most striking effects of the Renner-Teller interaction.

Jungen and Merer[20] explained the phenomenon of reordering by again considering the correlation between the vibronic energy levels of linear and bent molecules when $\Lambda \neq 0$. Such a correlation is illustrated in Fig. 4 for the specific case of $^{11}BH_2$. On the right-hand side, we have placed the experimental (or theoretical, they are the same at the resolution of the plot) $N = K$ levels (neglecting the effect of electron-spin and equating K with K_a) of the ground state of BH_2, taken from Table IV. The levels of the upper Renner-Teller component (the excited state) have been omitted for clarity. On the left-hand side, we have a schematic set of vibronic energy levels of a linear molecule in a $^1\Pi$ state with small Renner-Teller splittings, labeled by $K = |\pm\Lambda + l|$. Many of the possible levels with higher K have been omitted as they are not relevant to the discussion.

The energy levels on the left-hand side were carefully placed relative to those of bent BH_2 with two considerations in mind. First of all, well above the barrier to linearity, the energy level pattern approaches that of a linear molecule. Thus, the bent molecule levels must have energies similar to the energies of the linear molecule levels to which they correlate. Second, well above the barrier, the $A_{eff} = |K = 1 - K = 0|$ interval must be comparable to the vibrational frequency of the linear molecule, as described earlier.

Figure 4 shows that at low energies, the bent molecule has the typical asymmetric top pattern, which continues up

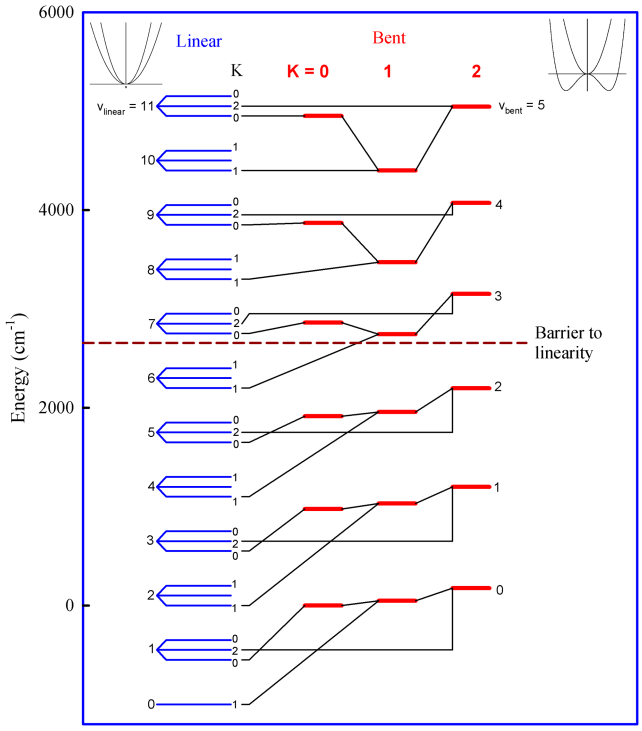

FIG. 4. Correlation of the measured $K = 0$–2 rovibronic levels for the ground state of $^{11}BH_2$ (right-hand side) with a hypothetical set of linear molecule $^1\Pi$ state vibronic levels (left hand side) in the limit of a small Renner-Teller effect. Only the lowest few K states are given for each linear molecule vibrational state and those which are not explicitly connected to bent state levels correlate instead with BH_2 excited state levels (not shown). The location of the barrier to linearity is given by the horizontal dashed line.

through $v_{bent} = 2$, just below the barrier to linearity. Well above the barrier, at $v_{bent} = 5$, both criteria discussed above are clearly met. In this region, the $K = 0$ and 2 levels correlate with $v_{linear} = 2v_{bent} + 1$, whereas the $K = 1$ levels correlate with $v_{linear} = 2v_{bent}$ which is one vibrational level lower so that $K = 1$ must fall below $K = 0$. In other words, the necessity that the bent molecule energy levels evolve into those of a linear molecule results in a reordering in the region just above the barrier and the $K = 1$ levels fall progressively below $K = 0$ for a given value of v_{bent}. Consideration of the correlation diagram for the upper Renner-Teller component[20] (in this case, the excited state) shows that there is no corresponding reordering effect.

Jungen and Merer[20] have shown that the reordering is a result of matrix elements that represent vibronic coupling *within* a Renner-Teller component. There are also "coupling" elements that act *between* components, perturbing levels with $K > 0$. Although these interactions between components have been suggested to be the cause of reordering of the lower levels,[23] in fact they are only subsidiary. Thus, in BH_2, the reordered $K = 1$ levels of the ground state can be further depressed by interactions with higher levels of the upper component, interactions that get stronger for near-coincidences of upper and lower state levels of the appropriate symmetry. Indeed, an examination of the wavefunctions from our BH_2 calculations shows that the ground state $K = 1$ levels up $v_{bent} = 7$ have a maximum of 18% excited state character at $v_{bent} = 4$ and only 11% for $v_{bent} = 5$, despite the much greater reordering in the latter.

If it were possible to follow the progress of the ground state bending levels to the point where they become embedded in the excited state manifold, one would expect that the perturbations would be random, as the interactions would then occur from above and below and, in some cases of near-resonances, would be very strong. In fact, in our previous LIF study, we were able to identify transitions to three such perturbed ground state levels whose locations were accurately pinpointed by our potential energy surface/rovibronic energy level calculations.[8]

VI. CONCLUSIONS

In the present experimental work, we have studied the bending levels of the ground state of $^{11}BH_2$ up to $v_2'' = 5$ through a combination of low resolution emission spectroscopy and high resolution stimulated emission spectroscopic measurements. The resulting data paint a roadmap of the rovibronic energy levels below, through, and above the calculated barrier to linearity and provide stringent tests of our own[8] and any future theoretical calculations of the rovibronic energy levels of the BH_2 free radical. Comparing our previous calculations[8] of the energy levels with the experimental results shows general overall agreement but exhibits some systematic discrepancies of a few cm^{-1}, especially at higher values of K_a''.

ACKNOWLEDGMENTS

The authors are very grateful to Fumie X. Sunahori and Mohammed Gharaibeh for preliminary work on the emission spectrum of BH_2. We also thank an anonymous reviewer for words of wisdom concerning reordering. This material is based upon work supported by the National Science Foundation under Grant No. CHE-1106338. R.T. acknowledges financial support from the University of Bologna.

[1] G. Herzberg and J. W. C. Johns, Proc. R. Soc. A **298**, 142 (1967).
[2] M. Vervloet and J. K. G. Watson, J. Mol. Spectrosc. **217**, 255 (2003), and references therein.
[3] A. Shayesteh, K. Tereszchuk, P. F. Bernath, and R. Colin, J. Chem. Phys. **118**, 3622 (2003).
[4] L. B. Knight, M. Winiski, P. Miller, C. A. Arrington, and D. Feller, J. Chem. Phys. **91**, 4468 (1989).
[5] M. Peric, S. D. Peyerimhoff, and R. J. Buenker, Can. J. Chem. **59**, 1318 (1981).
[6] M. Brommer, P. Rosmus, S. Carter, and N. C. Handy, Mol. Phys. **77**, 549 (1992).
[7] M. Kolbuszewski, P. R. Bunker, W. P. Kraemer, G. Osmann, and P. Jensen, Mol. Phys. **88**, 105 (1996).
[8] F. X. Sunahori, M. Gharaibeh, D. J. Clouthier, and R. Tarroni, J. Chem. Phys. **142**, 174302 (2015).
[9] H. Harjanto, W. W. Harper, and D. J. Clouthier, J. Chem. Phys. **105**, 10189 (1996).
[10] M. A. Gharaibeh, R. Nagarajan, D. J. Clouthier, and R. Tarroni, J. Chem. Phys. **142**, 014305 (2015).
[11] S. Gerstenkorn and P. Luc, *Atlas du Spectre D'Absorption de la Molecule d'Iode* (Editions du C.N.R.S., Paris, 1978); Rev. Phys. Appl. **14**, 791 (1979).
[12] F. J. Northrup and T. J. Sears, Annu. Rev. Phys. Chem. **43**, 127 (1992).
[13] M. J. Frisch, G. W. Trucks, H. B. Schlegel *et al.*, GAUSSIAN 09, Revision C.02, Gaussian, Inc., Wallingford, CT, 2004.
[14] A. D. Becke, J. Chem. Phys. **98**, 5648 (1993).
[15] C. Lee, W. Yang, and R. G. Parr, Phys. Rev. B **37**, 785 (1988).
[16] T. H. Dunning, Jr., K. A. Peterson, and A. K. Wilson, J. Chem. Phys. **114**, 9244 (2001).
[17] A. Hoy, I. Mills, and G. Strey, Mol. Phys. **24**, 1265 (1972).
[18] J. W. C. Johns, Can. J. Phys. **45**, 2639 (1967).
[19] R. N. Dixon, Trans. Faraday Soc. **60**, 1363 (1964).
[20] Ch. Jungen and A. J. Merer, in *Molecular Spectroscopy, Modern Research*, edited by K. Narahari Rao (Academic, New York, 1976), Vol. II, p. 127.
[21] Ch. Jungen, D. N. Malm, and A. J. Merer, Can. J. Phys. **51**, 1471 (1973).
[22] Ch. Jungen and A. J. Merer, Mol. Phys. **40**(1), 95 (1980).
[23] P. R. Bunker and P. Jensen, *Molecular Symmetry and Spectroscopy*, 2nd ed. (National Research Council of Canada Press, Ottawa, 2006).